

Published in final edited form as:

Phys Chem Chem Phys. 2019 April 17; 21(16): 8197–8200. doi:10.1039/c9cp00634f.

Endohedral metal-nitride cluster ordering in metallofullerene–Ni^{II}(OEP) complexes and crystals: a theoretical study†

Vasilii Dubrovin^a, Li-Hua Gan^{a,b}, Bernd Büchner^a, Alexey A. Popov^{iD,*,a}, Stanislav M. Avdoshenko^{iD,*,a}

^aIFW Dresden, Helmholtzstraße 20, 01069 Dresden, Germany

^bSchool of Chemistry and Chemical Engineering, Southwest University, Chongqing 400715, China

Abstract

The ordering of endohedral clusterfullerenes Sc₃N@C₈₀ and YSc₂N@C₈₀ co-crystallized with Ni(OEP) and isolated complexes with Ni(OEP) have been investigated theoretically. Having used multiple orientations of M₃N clusters inside the cages with Fibonacci sampling, we describe the effect of intermolecular interactions on the orientation of the endohedral cluster.

Molecules of fullerenes encapsulating metal atoms or clusters (*aka* endohedral metallofullerenes, EMFs¹) can be considered as molecular ball-bearings or gyroscopes consisting of two semi-independent structural units. Despite the strong interactions between the metal atoms and fullerene π -system, the potential energy surface for the rotation of the clusters inside the cages is often rather shallow, leading to quasi-free rotations of endohedral species. A prominent example is found in nitride clusterfullerenes M₃N@C₈₀-I_h, where M can be Sc, Y, lanthanides, or any combination of them.² The icosahedral C₈₀ cage is almost a sphere with many equivalent bonding sites for metal atoms. NMR spectroscopy confirms that in solutions the M₃N cluster rotates freely at room temperature.³ For Sc₃N@C₈₀, early computational studies have predicted the barrier to this rotation to be below 10 kJ mol⁻¹,⁴ and similar estimations have been made based on STM⁵ and NMR measurements.⁶ Obtaining ordered assemblies of such molecules in crystals or in layered structures on surfaces is a challenging task, which, however, may have a high practical impact because the orientation of endohedral clusters affects the electronic and magnetic properties of EMF materials. Furthermore, molecular structure determination by single-crystal X-ray diffraction is complicated by a severe disorder caused by a loosely bound endohedral cluster and rotation of the fullerene cage itself.

Alexey A. Popov: 0000-0002-7596-0378

Stanislav M. Avdoshenko: 0000-0001-5839-3079

This article is licensed under a [Creative Commons Attribution 3.0 Unported Licence](https://creativecommons.org/licenses/by/3.0/).

a.popov@ifw-dresden.de, s.avdoshenko@gmail.com.

Conflicts of interest

There are no conflicts to declare.

Early in the days it was noticed that empty fullerenes would not rotate as freely if they were captured in non-covalent complexes as co-crystals.⁸ This way a precise molecular structure of many fullerenes got to be known with a little to no disorder.⁹ In modern EMF research, co-crystallization of EMFs with metal-octaethylporphyrin ($\text{Me}^{\text{II}}(\text{OEP})$, $\text{Me}^{\text{II}} = \text{Ni}$ or Co)¹⁰ has become a *de facto* standard for X-ray diffraction studies.¹¹ For nitride clusterfullerenes $\text{M}_3\text{N}@C_{80}\text{-}I_h$, it turns out that not only has the cage been subdued to order by the presence of $\text{Me}(\text{OEP})$, but also the inner nitride clusters.¹² It was also found that the orientation of the M_3N cluster is very sensitive to its exact composition – be it monoionic Sc_3N or a mixed-metal LnSc_2N system with $\text{Ln} = \text{La}, \text{Ce}, \text{Gd}, \text{Tb}, \text{Er}, \text{or Dy}$.^{7,13} Taking into account a very low barrier of inner rotation for the M_3N clusters, this is a remarkable observation of great importance in EMF chemistry. Although the ordering effect has already been known for years, it would be fair to say that its origin is still not well understood. However, it would be of great use to know the exact energy scale of the effect and if it has a local or cooperative nature to strategize the search for and design of EMF materials as the ability to form ordered arrays is an important criterion.

In this communication, we explore the influence of the interaction between $\text{M}_3\text{N}@C_{80}$ and $\text{Ni}(\text{OEP})$ on the orientation of the endohedral cluster by comprehensive computational studies. To study the EMF– $\text{Ni}(\text{OEP})$ interaction in different environments, we design two sets of systems: (I) co-**CR**ystals (**CRS- x** , $x = 0, 1$) of $\text{Y}_x\text{Sc}_{3-x}\text{N}@C_{80}$ with $\text{Ni}(\text{OEP})$ in the experimental crystal settings taken from ref. 7 (Fig. 1a) and (II) **CO**mplex **SE**t (**COS- x** , $x = 0, 1$) with the isolated $\text{Y}_x\text{Sc}_{3-x}\text{N}@C_{80}\text{-Ni}(\text{OEP})$ molecular complexes. Since the ionic radius of Y is close to those of a set of lanthanides (Tb, Dy, Ho, *etc.*), the results obtained in this work for $\text{YSc}_2\text{N}@C_{80}$ are representative of a larger group of $\text{MSc}_2\text{N}@C_{80}$ compounds, including those with magnetic lanthanide atoms. Computations were done using the VASP5.0 code at the PBE-D3/PAW level of theory with a plane-wave basis cut-off of 400 eV consistent with the pseudopotential.^{†14}

The endohedral cluster in the isolated $\text{M}_3\text{N}@C_{80}\text{-}I_h$ molecule has 2–3 energy minima with small energy differences. Obviously, the interaction of the EMF molecule with $\text{Ni}(\text{OEP})$ changes this situation, else the ordering effect would not be observed experimentally. In other words, the potential energy surface (PES) for the cluster inside the cage becomes more prolific when it interacts with $\text{Ni}(\text{OEP})$ with the appearance of pronounced orientational minima. But since EMF– $\text{Ni}(\text{OEP})$ interactions are non-bonded, the energetic effect on the endohedral cluster cannot be very strong. To make the theoretical depiction of the systems complete and consistent, it is necessary to ensure that all energy minima corresponding to the different orientations of the cluster inside the fullerene are found. It would be insufficient to optimize one particular structure with an arbitrary orientation of the endohedral cluster. As illustrated schematically in Fig. 1b, for the complex PES as a function of the order parameter θ , with multiple energy minima, a single optimization will most probably proceed into the closest energy minimum in the configurational space (Fig. 1b, the green dot and

[†]Each system was optimized to a residual force of $0.005 \text{ \AA}^{-1} \text{ eV}^{-1}$. All optimizations for crystal and molecular systems were performed at the Γ -point. The molecular systems were put in a cubic unit cell with a side of 25 \AA , which ensures no impact due to interactions with periodic images. The results were analyzed and visualized with in-house Python scripts.¹⁷ Molecular structures are visualized with the VMD package.¹⁸

trajectory line), and not necessarily into the global energy minimum. Only if the configurational space is properly sampled (Fig. 1b, all starting points and trajectories), the reliable reconstruction of the PES minima is feasible. Exhaustive and regular sampling of the orientational phase space is achieved here by the Fibonacci sphere sampling. Namely, for each system 120 conformational isomers were generated by rotating the internal cluster along the Fibonacci sphere with respect to the nitrogen as shown for **CRS-0** in Fig. 1. Herewith one of the Sc atoms in $\text{Sc}_3\text{N@C}_{80}$ or the Y atom in $\text{YSc}_2\text{N@C}_{80}$ walks over the sphere, while the M_3N cluster is kept rigid through relevant rotation in polar coordinates (see the ESI† for generation script). The angle between the M–N bond and the Z-axis defines the order parameter θ (Fig. 1). Since each conformer tends to relax to the closest minimum, insufficient and/or biased sampling may lead to unfair judgments about the energy minima distribution. The proposed homogenous sampling ensures maximum conformation space coverage for a given number of nodes.

At first, the outlined computational approach is applied for the isolated $\text{Sc}_3\text{N@C}_{80}$ molecule. Fig. 2a shows the energy distributions of the optimized conformers. Optimization of all 120 initial structures generated by Fibonacci sampling results in only two real minima with C_3 and C_s symmetry (see Fig. S1 of the ESI†) in agreement with earlier DFT studies.⁴ The energy difference between the two structures is only 2.3 kJ mol^{-1} , which is consistent with the free rotation of Sc_3N within C_{80} at room temperature. For an isolated $\text{YSc}_2\text{N@C}_{80}$ molecule, the procedure resulted in 3 unique structures (Fig. 2d, and Fig. S2 of the ESI†) with relative energies of 0, 2.6, and 3.8 kJ mol^{-1} .

For the **CRS** and **COS** groups (Fig. 2), the energy distributions of the optimized structures still have a narrow energy spread ($\Delta E \approx 16 \text{ kJ mol}^{-1}$). However, these narrow ranges are visibly larger than those in the isolated $\text{Sc}_3\text{N@C}_{80}$ and $\text{YSc}_2\text{N@C}_{80}$ molecules, which illustrates the effect of intermolecular interactions on the orientation of the M_3N cluster. The most stable structures in all cases are consistent with experimental observations. For example, in the **CRS-1** and **COS-1** systems, the Y atom is placed remotely to the Ni-site. However, the energy differences of energetically close conformers are minuscule. Therefore, in the window of $1k_B T$ at room temperature (2.5 kJ mol^{-1}), one would find up to 10 conformers (as in the case of **CRS-0**). Nevertheless, structurally, these minima are very similar to the global minimum.

Let's consider the **COS** and **CRS** groups in more detail. When the $\text{M}_3\text{N@C}_{80}$ molecule is set to interact with Ni(OEP), the energy distribution of the optimized structures changes considerably. Instead of 2–3 unique minima found for the isolated $\text{M}_3\text{N@C}_{80}$ molecules, calculations predict the appearance of multiple different minima in the **COS-0,1** structures. This shows that the non-covalent interaction with Ni(OEP) breaks the orientation isotropy of the icosahedral fullerene cage. Second, the ΔE spread of the **COS** structures ($\sim 12 \text{ kJ mol}^{-1}$) is increased four-fold in comparison to the isolated $\text{Sc}_3\text{N@C}_{80}$ and $\text{YSc}_2\text{N@C}_{80}$ molecules. These differences between $\text{M}_3\text{N@C}_{80}$ molecules and **COS** systems clearly point to the considerable effect of the intermolecular interaction on the orientation of the endohedral cluster in $\text{M}_3\text{N@C}_{80}\cdot\text{Ni(OEP)}$ complexes.

The lowest energy conformers in **COS-0,1** are grouped near $\theta = 0$, which corresponds to the vertical orientation of the Sc–N or Y–N bond remotely from the Ni(OEP)-coordination site of the fullerene cage (Fig. 2c and d). Two other Sc–N bonds are oriented towards the Ni(OEP) molecule. This orientation of the endohedral cluster corresponds to the experimentally observed orientation in $M_3N@C_{80}\cdot Ni(OEP)$ crystals.^{7,13}

The cluster composition plays an important role in the overall energy distribution. Since the Sc–N–Sc angle is close to $2\pi/3$, stable **COS-0** conformers can also be obtained for $\theta = 2\pi/3$ (in this case another Sc atom has a vertical orientation). Indeed, clustering of low-energy conformers can be seen near $\theta = 2\pi/3$. In total, the energy distribution of the **COS-0** conformers is very dense, giving only a moderate ordering effect for the energy cut-off of $1k_B T$ at room temperature. For the YSc_2N cluster in the **COS-1** system, the situation is different. The conformer with $\theta = 0$ corresponds to the well-defined global minimum. If the positions of Y and one Sc atom are flipped (giving $\theta = 2\pi/3$), the energies increase by *ca.* 5 kJ mol^{-1} . Thus, the ordering effect for $YSc_2N@C_{80}\cdot Ni(OEP)$ is more pronounced and gives essentially one structure for the energy cut-off of $E = 2.5 \text{ kJ mol}^{-1}$.

When $M_3N@C_{80}\cdot Ni(OEP)$ complexes are placed in a crystalline environment, the energy distributions in the **CRS-0,1** systems resemble those of **COS-0,1**, but with noticeable alterations. First, the relative energy spread is increased further by *ca.* 25–30%. Second, the stability of the conformers near $\theta = 0$ and $\theta = 2\pi/3$ is enhanced in **CRS-0** compared to **COS-0**. Thus, the ordering effect on the Sc_3N cluster is stronger in the crystal than in the isolated $Sc_3N@C_{80}\cdot Ni(OEP)$ complex. Third, for **CRS-1** the crystalline environment enhances the relative stability of the conformers with $\theta = 2\pi/3$. The conformer with the vertical orientation of the Y–N bond ($\theta = 0$) is still the most stable, but the structure with the flipped positions of Y and Sc is only 2.5 kJ mol^{-1} higher. Thus, the crystalline environment enhances the preferential orientation of the nitride clusters but makes the Y and Sc positions in $YSc_2N@C_{80}$ less energetically different. This agrees with our recent study of $DYSc_2N@C_{80}\cdot Ni(OEP)$ crystals,⁷ which showed that the vertical orientation of the Dy–N bond was more preferable, but the site with the flipped Sc and Dy positions had up to ~20% occupancy in one of the crystal batches.

As both Ni(OEP) and EMF molecules have inhomogeneous charge distribution, electrostatic interactions may play an important role. This factor can be analyzed qualitatively with the help of electrostatic potential distribution¹⁵ as shown in Fig. 3. The nitrogen atoms in Ni(OEP) create a rather high negative potential. To achieve optimal electrostatic interactions, an EMF molecule should be oriented towards Ni(OEP) with its highest positive potential sites. As shown in Fig. 3 for $YSc_2N@C_{80}$, the poles of the cage have a more negative potential as opposed to the Sc- or Y-coordination sites on the equator, where the potential is more positive. The highest relative energies are indeed found for those structures, in which the pole of the EMF faces Ni(OEP) (*i.e.* the M_3N cluster is aligned parallel to the Ni(OEP), θ near $\pi/2$), whereas in the lowest energy structures two metal atoms of the cluster face Ni(OEP). Note that the positive potential around the Sc-binding sites is slightly higher than that for the Y-binding site (Fig. 3), which may explain why the vertical orientation of the Y–N bond is preferable in $YSc_2N@C_{80}\cdot Ni(OEP)$.

To pinpoint the energetic contributions which govern the effect, we analyze the classical dispersion and Coulomb interactions in the **COS-0** system. The dispersion is evaluated according to Grimme's model (D3).^{14d} Electrostatic interactions were evaluated with absolutely-localized molecular orbital energy decomposition analysis (ALMO EDA) as implemented in the Q-chem4.4 code.¹⁶ The results are summed up in Fig. 4. The median of the relative dispersion energy in the **COS-0** set is close to 2.5 kJ mol⁻¹ with no preference for any particular value of θ (Fig. 4 (G)). Differently, the frozen density Coulomb repulsion energy gives a stronger discrimination of the conformers and is able to indicate a few of the most stable structures. However, not all stable structures would be selected based on this criterion, as it appears from the direct comparison in Fig. 4. This discrepancy comes from more complex interactions and cannot be accounted for within the ALMO EDA model, which focuses on electrostatic effects, *e.g.*, charge–charge, charge–dipole, and charge–induced dipole interactions. Moreover, an additional discrepancy can arise due to the lack of long-range Coulomb interactions in the current ALMO EDA model.

To summarize, DFT calculations at the PBE-D3 level provided a reliable description of M₃N@C₈₀·Ni(OEP) systems and revealed how non-covalent interactions with Ni(OEP) result in a substantial ordering effect for the endohedral cluster in Sc₃N@C₈₀ and YSc₂N@C₈₀ molecules. Assuming thermodynamic control with thermal averaging over 2.5 kJ mol⁻¹ (RT), the nitride clusters are predicted to be well ordered. However, the energy scale of this effect is rather narrow, and the ordering will disappear if the thermal energy range covers $E = 10$ kJ mol⁻¹. The results on YSc₂N@C₈₀·Ni(OEP) can be generalized to other EMFs with a middle-sized lanthanide in place of Y.

Supplementary Material

Refer to Web version on PubMed Central for supplementary material.

Acknowledgments

The authors acknowledge funding by the Marie Skłodowska-Curie actions (EU project 'SamSD' to SA, grant agreement no. 748635), the European Research Council under the European Union's Horizon 2020 research and innovation program (grant agreement no. 648295 'GraM3' to AAP), and the National Natural Science Foundation of China (grant no. 51472208 to LHG). Computational resources were provided by ZIH at TU Dresden.

References

1. (a) Popov AA, Yang S, Dunsch L. *Chem Rev.* 2013; 113:5989. [PubMed: 23635015] (b) Yang S, Wei T, Jin F. *Chem Soc Rev.* 2017; 46:5005. [PubMed: 28681052]
2. Zhang J, Stevenson S, Dorn HC. *Acc Chem Res.* 2013; 46:1548. [PubMed: 23489255]
3. Zhang J, Dorn HC. *Fullerenes, Nanotubes, Carbon Nanostruct.* 2014; 22:35.
4. Popov AA, Dunsch L. *J Am Chem Soc.* 2008; 130:17726. [PubMed: 19035640]
5. Huang T, Zhao J, Feng M, Popov AA, Yang S, Dunsch L, Petek H. *Nano Lett.* 2011; 11:5327. [PubMed: 22081996]
6. Fu W, Wang X, Azuremendi H, Zhang J, Dorn HC. *Chem Commun.* 2011; 47:3858.
7. Krylov D, Liu F, Brandenburg A, Spree L, Bon V, Kaskel S, Wolter A, Buchner B, Avdoshenko S, Popov AA. *Phys Chem Chem Phys.* 2018; 20:11656. [PubMed: 29671443]
8. (a) Neretin IS, Slovokhotov YL. *Russ Chem Rev.* 2004; 73:455. (b) Konarev DV, Lyubovskaya RN. *Usp Khim.* 1999; 68:23.

9. (a) Michel RH, Kappes MM, Adelman P, Roth G. *Angew Chem, Int Ed Engl.* 1994; 33:1651. (b) Ziegler K, Amsharov KY, Halasz I, Jansen M. *Z Anorg Allg Chem.* 2011; 637:1463. (c) Eppler L, Amsharov K, Simeonov K, Dix I, Jansen M. *Chem Commun.* 2008:5610. (d) Balch AL, Olmstead MM. *Coord Chem Rev.* 1999; 186:601. (e) Yang H, Mercado BQ, Jin H, Wang Z, Jiang A, Liu Z, Beavers CM, Olmstead MM, Balch AL. *Chem Commun.* 2011; 47:2068. (f) Yang H, Beavers CM, Wang Z, Jiang A, Liu Z, Jin H, Mercado BQ, Olmstead MM, Balch AL. *Angew Chem, Int Ed.* 2010; 49:886. (g) Wang Z, Yang H, Jiang A, Liu Z, Olmstead MM, Balch AL. *Chem Commun.* 2010; 46:5262.
10. Olmstead MM, Costa DA, Maitra K, Noll BC, Phillips SL, Van Calcar PM, Balch AL. *J Am Chem Soc.* 1999; 121:7090.
11. (a) Stevenson S, Rice G, Glass T, Harich K, Cromer F, Jordan MR, Craft J, Hadju E, Bible R, Olmstead MM, Maitra K, et al. *Nature.* 1999; 401:55. (b) Svitova AL, Ghiassi K, Schlesier C, Junghans K, Zhang Y, Olmstead M, Balch A, Dunsch L, Popov AA. *Nat Commun.* 2014; 5:3568. [PubMed: 24699547] (c) Jin H, Yang H, Yu M, Liu Z, Beavers CM, Olmstead MM, Balch AL. *J Am Chem Soc.* 2012; 134:10933. [PubMed: 22536841] (d) Mercado BQ, Chen N, Rodriguez-Fortea A, Mackey MA, Stevenson S, Echegoyen L, Poblet JM, Olmstead MM, Balch AL. *J Am Chem Soc.* 2011; 133:6752. [PubMed: 21473581] (e) Yang S, Chen C, Liu F, Xie Y, Li F, Jiao M, Suzuki M, Wei T, Wang S, Chen Z, Lu X, et al. *Sci Rep.* 2013; 3:1487. [PubMed: 23512079] (f) Shen W, Bao LB, Hu S, Gao X, Xie Y, Gao X, Huang W, Lu X. *Chem – Eur J.* 2018; 24:16692. [PubMed: 30221415] (g) Shen W, Bao L, Wu Y, Pan C, Zhao S, Fang H, Xie Y, Jin P, Peng P, Li F, Lu X. *J Am Chem Soc.* 2017; 139:9979. [PubMed: 28679207] (h) Kurihara H, Lu X, Iiduka Y, Nikawa H, Hachiya M, Mizorogi N, Slanina Z, Tsuchiya T, Nagase S, Akasaka T. *Inorg Chem.* 2012; 51:746. [PubMed: 22148556]
12. Olmstead MM, Zuo T, Dorn HC, Li T, Balch AL. *Inorg Chim Acta.* 2017; 468:321.
13. (a) Stevenson S, Rose CB, Maslenikova JS, Villarreal JR, Mackey MA, Mercado BQ, Chen K, Olmstead MM, Balch AL. *Inorg Chem.* 2012; 51:13096. [PubMed: 23214426] (b) Olmstead MM, de Bettencourt-Dias A, Duchamp JC, Stevenson S, Dorn HC, Balch AL. *J Am Chem Soc.* 2000; 122:12220. (c) Wang XL, Zuo TM, Olmstead MM, Duchamp JC, Glass TE, Cromer F, Balch AL, Dorn HC. *J Am Chem Soc.* 2006; 128:8884. [PubMed: 16819883] (d) Stevenson S, Chancellor C, Lee HM, Olmstead MM, Balch AL. *Inorg Chem.* 2008; 47:1420. [PubMed: 18247561] (e) Krylov DS, Liu F, Avdoshenko SM, Spree L, Weise B, Waske A, Wolter AUB, Büchner B, Popov AA. *Chem Commun.* 2017; 53:7901.
14. (a) Kresse G, Hafner J. *Phys Rev B: Condens Matter Mater Phys.* 1993; 47:558. (b) Kresse G, Joubert D. *Phys Rev B: Condens Matter Mater Phys.* 1999; 59:1758. (c) Perdew JP, Burke K, Ernzerhof M. *Phys Rev Lett.* 1996; 77:3865. [PubMed: 10062328] (d) Grimme S. *WIREs Comput Mol Sci.* 2011; 1:211.
15. (a) Yang H, Wang Z, Jin H, Hong B, Liu Z, Beavers CM, Olmstead MM, Balch AL. *Inorg Chem.* 2013; 52:1275. [PubMed: 23343255] (b) Yang H, Jin H, Wang X, Liu Z, Yu M, Zhao F, Mercado BQ, Olmstead MM, Balch AL. *J Am Chem Soc.* 2012; 134:14127. [PubMed: 22860880] (c) Stania R, Seitsonen AP, Kunhardt D, Büchner B, Popov AA, Muntwiler M, Greber T. *J Phys Chem Lett.* 2018; 9:3586. [PubMed: 29902014]
16. Shao Y, Gan Z, Epifanovsky E, Gilbert ATB, Wormit M, Kussmann J, Lange AW, Behn A, Deng J, Feng X, Ghosh D, et al. *Mol Phys.* 2015; 113:184.
17. Ask Hjorth L, Jens Jørgen M, Jakob B, Ivano EC, Rune C, Marcin D, Jesper F, Michael NG, Bjørk H, Cory H, Eric DH, et al. *J Phys: Condens Matter.* 2017; 29:273002. [PubMed: 28323250]
18. Humphrey W, Dalke A, Schulten K. *J Mol Graphics.* 1996; 14:33.

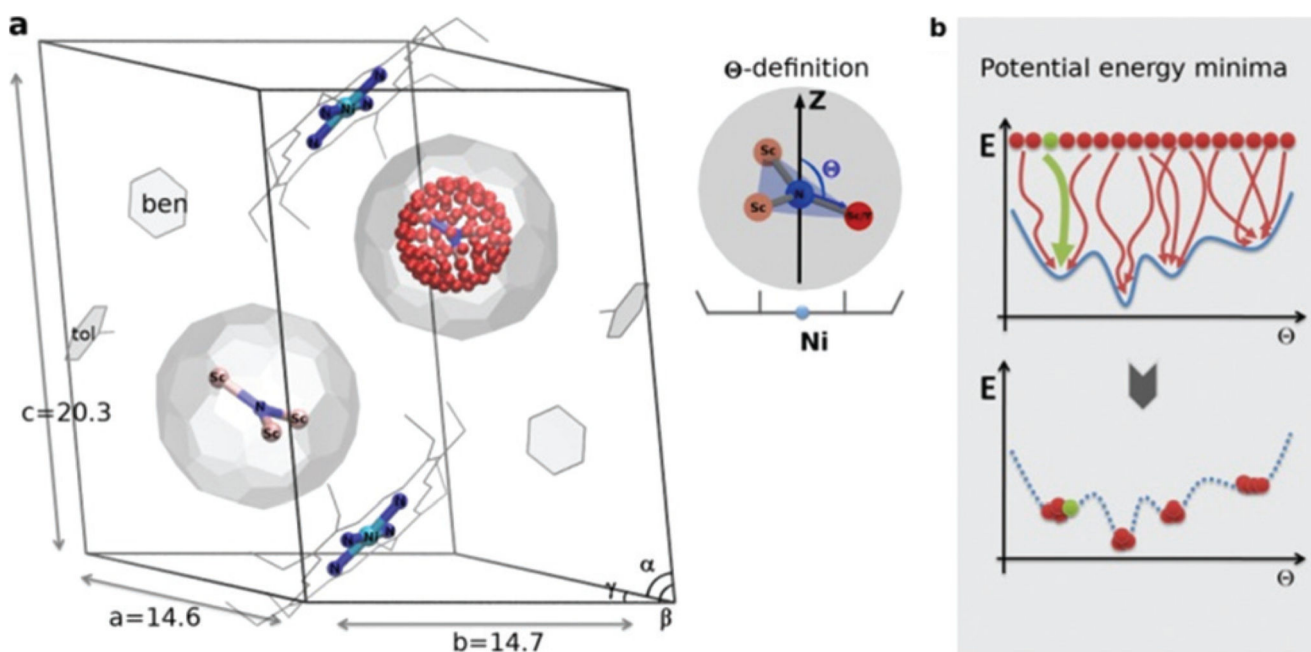


Fig. 1.

(a) $\text{Sc}_3\text{N}@C_{80}\cdot\text{Ni}^{\text{II}}(\text{OEP})$ crystal system used in the theoretical study, based on the X-ray data in ref. 7. In one fullerene cage the Sc_3N cluster is rotated along the Fibonacci sphere with sampling 120-nodes. In the second cage the Sc_3N cluster has a natural orientation. The order parameter θ is defined as an angle between the atomic position captured in red and the Z -axis (black arrow). (b) Schematic illustration of potential energy minima reconstruction based on homogenous sampling (see text for details).

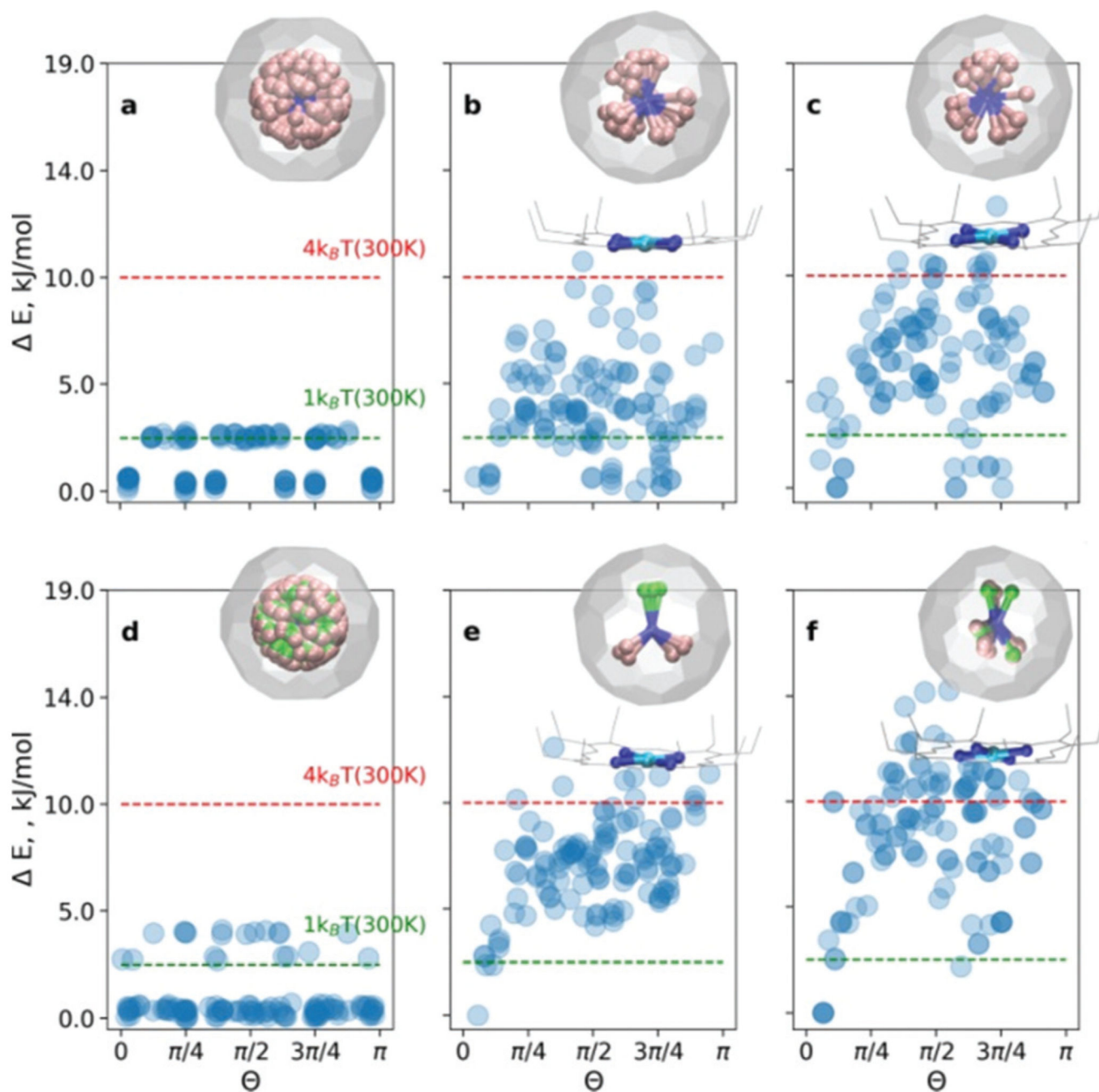


Fig. 2. Relative energy distributions as a function of the order parameter Θ for (a and d) isolated $\text{Sc}_3\text{N}@C_{80}$ and $\text{YSc}_2\text{N}@C_{80}$, (b and e) complex systems (COS-0, COS-1) and (c and f) crystal systems (CRS-0, CRS-1), respectively. The right upper corner graphics show superposed structures with $E < 2.5 \text{ kJ mol}^{-1}$.

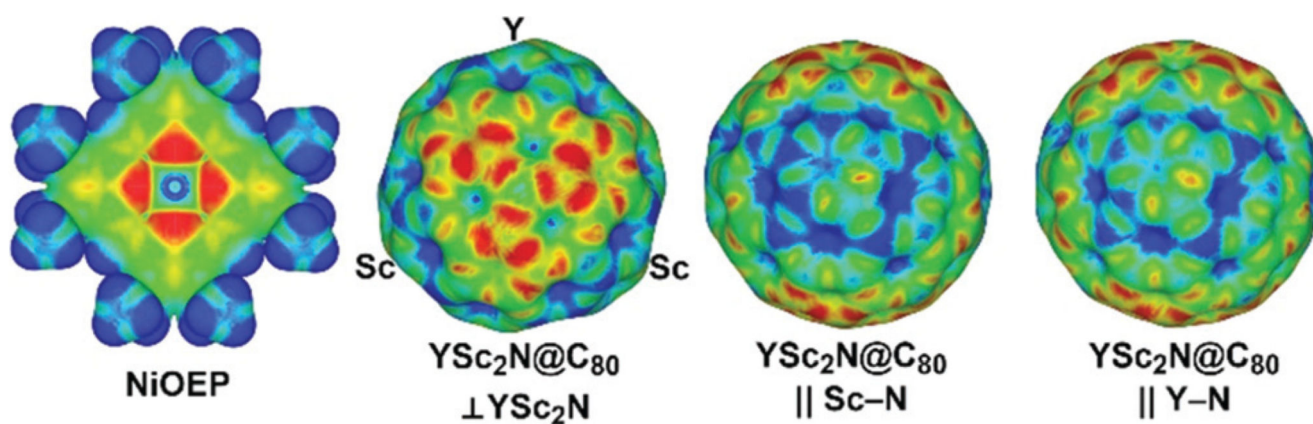


Fig. 3. Electrostatic potentials in Ni(OEP) and YSc₂N@C₈₀ molecules (red and blue indicate more negative and positive potentials, respectively) mapped on the electron density isosurface of 0.01 a.u. YSc₂N@C₈₀ is shown in three orientations: normal to the YSc₂N plane and along the Sc-N and Y-N bonds.

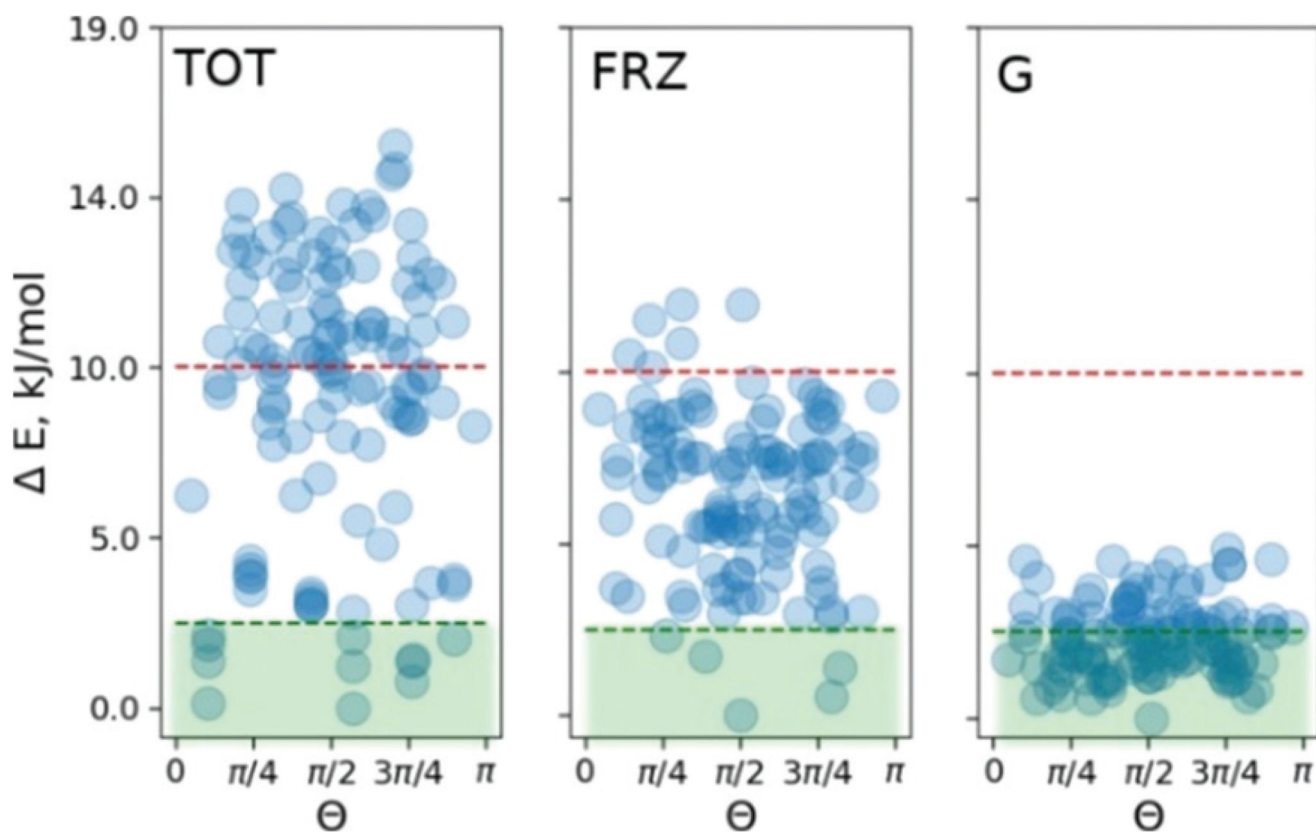


Fig. 4. ALMO energy decomposition for the **COS-0** set. TOT, distribution of the total energy at the PBE/6-31G* level of theory; FRZ, frozen density Coulomb interaction energy between $\text{Sc}_3\text{N}@C_{80}$ and Ni(OEP) fragments; and G, Grimme's dispersion energy.